JOURNAL OF GUIDANCE, CONTROL, AND DYNAMICS
Vol. 32, No. 3, May–June 2009

Analytical Assessment of Flight Simulator Fidelity Using Pilot Models

Ronald A. Hess*
University of California, Davis, Davis, California 95616
and
Federico Marchesi†
Università degli Studi di Brescia, 25121 Brescia (Lombardie), Italy

DOI: 10.2514/1.40645

A simplified approach for modeling pilot pursuit control behavior is adopted for use in assessing the fidelity of flight simulators. The model includes proprioceptive, visual, and vestibular cueing. The model differs from previous simulator fidelity applications in that pursuit, as opposed to compensatory pilot behavior, is modeled. In approximate fashion, the model can account for the effects of task interference, degraded motion and visual cues, vehicle modeling errors, differing levels of pilot control aggressiveness, and to a limited extent, pilot skill level. A fidelity metric similar to one previously discussed in the literature is exercised with three vehicles and tasks: a fighter aircraft in a tail-chase tracking task, a small rotorcraft in a near-hover repositioning task, and a large rotorcraft in acceleration/deceleration and departure/abort tasks. The fidelity assessment procedure is shown to be sensitive to changes in vehicles, tasks, and simulator limitations in these disparate examples.

Nomenclature

$dvar_{\text{task}}$	=	variance of band-limited white noise in visual cue model associated with piloting task
$dvar_{\text{vis}}$	=	variance of band-limited white noise in visual cue model associated with visual cue quality
f	=	$1 + 10(dvar_{\text{vis}} + dvar_{\text{task}})$ factor in pilot model related to visual cue quality and task interference
G_{nm}	=	neuromotor system dynamics in pilot model
h	=	vehicle altitude
K_p	=	pilot model gain in inner "position" control loop
K_{po}	=	pilot model gain in outer position control loop, multi-axis task
K_r	=	pilot model gain in inner "rate" control loop
K_{ro}	=	pilot model gain in outer rate control loop, multi-axis task
k_{agress}	=	pilot model gain to model pilot control aggressiveness in a task
$k_{(\,)}$	=	pilot model gain on variable ( )
$L'_{\delta_{(\,)}}$	=	moment-normalized stability derivative relating primed rolling moment to control input $\delta_{(\,)}$
M	=	output of inner position control loop
$M_{\delta_{(\,)}}$	=	moment-normalized stability derivative relating pitching moment to control input $\delta_{(\,)}$
n	=	number of axes being controlled by pilot
$P_i(\omega)_{\text{nom}}$	=	power in ith proprioceptive feedback loop, nominal conditions (without simulator limitations)
$P_i(\omega)_{\text{sim}}$	=	power in ith proprioceptive feedback loop, nominal conditions (with simulator limitations)
p	=	vehicle roll rate, deg/s
q	=	vehicle pitch rate, deg/s
r	=	vehicle yaw rate, deg/s
UM	=	proprioceptive feedback signal
V	=	vehicle velocity
x, y	=	vehicle longitudinal and lateral positions in Earth-fixed axes
Y_p	=	pilot model transfer function
δ_A	=	pilot's lateral cyclic input
δ_B	=	pilot's longitudinal cyclic input
θ	=	vehicle pitch attitude, deg
ϕ	=	vehicle roll attitude, deg
ψ	=	vehicle heading, deg

I. Introduction

APPLYING techniques for modeling the control behavior of the human pilot has been of considerable interest in assessing flight simulator fidelity [1–12]. The research to be discussed here will focus upon a simplified model of pilot behavior introduced in [13], and further exercised in [14]. The goal of the simplification is to reduce the complexity of the model used in previous studies [6], while still retaining desirable features amenable to application to fidelity studies. The modeling approach to be presented is directed primarily toward establishing flight simulator requirements for training. In particular, a procedure will be proposed that will attempt to quantify the effects of specific simulator limitations and do so while accommodating the particular vehicle and flight task being simulated. The critical element in this analytical assessment will be a pilot model that includes the primary sensory paths that the human used in controlling a vehicle, that is, visual, proprioceptive, and vestibular. In comparison to past work dealing with flight simulator fidelity, the methodology to be discussed follows a number of well-defined, sequential steps that are of particular help in determining the dynamics of the so-called "proprioceptive" control loop of the human [15]. The need for more automated tuning of pilot models that have been proposed in the past for simulator fidelity assessment has been pointed out by others [11] and is critical in modeling realistic flight tasks such as those studied in [16]. In addition to accommodating the cues just described, the pilot model includes an approximate means for accounting for the effects of interference in multiloop control tasks, a feature that was absent in previous fidelity studies [6]. To exercise the proposed methodology, it is applied to three different vehicles (fighter aircraft, small rotorcraft, and large rotorcraft) in significantly different piloting tasks. The tasks are 1) a fighter tail chase at Mach = 0.3, 2) a small rotorcraft near-hover task, and 3) two tasks with a large rotorcraft involving significant ground-

Presented as Paper 6682 at the AIAA Modeling and Simulation Techologies Conference, Honolulu, Hawaii, 18–21 August 2008; received 27 August 2008; revision received 27 December 2008; accepted for publication 30 December 2008.

*Professor, Department of Mechanical and Aeronautical Engineering. Associate Fellow AIAA.
†Student, Dipartimento di Elettronica per l'Automazione.

speed changes from hover. By applying the methodology to these disparate vehicles and tasks, the authors hope to emphasize the broad applicability of the technique.

The paper is organized as follows. Section II discusses the pilot model which is the central element in the methodology. The section discusses how the model is created for any vehicle and task and concludes with the procedure offered for quantifying simulator fidelity. Section III presents an application of the fidelity assessment procedure to a tail-chase task with a fighter aircraft. Section IV treats a near-hover task with a small rotorcraft. Section V applies the technique to a large rotorcraft in a pair of tasks in which time-varying vehicle dynamics are encountered. Section VI comprises a discussion and critique of the assessment procedure and Sec. VII draws the major conclusions from the study.

II. Pilot Model

A. Basic Structure

The work of Hess in [13] describes the core of the pilot modeling procedure to be discussed herein. The work of Hess [13] was motivated by a desire to provide tractable pilot models for inclusion in computer simulations of realistic and demanding piloting tasks. The brief description that follows is essentially identical to that offered in [13,14]. The pilot model is multiloop in nature, with each sequential loop described by an inner (rate) and outer (position) closure. Here rate and position are used in a relative sense. All that is intended in this description is that the inner-loop response variable is the time derivative of the outer-loop response variable. Figure 1 shows the model structure for the innermost loop in a flight control task. In this discussion, "innermost" control loop will refer to the feedback loop that produces direct control inputs by the pilot through the cockpit inceptor. Beginning with such an innermost control loop, each vehicle response variable is controlled using a combination of output-rate feedback ($\dot{M}$) and output feedback (M). Each of these separate feedback loops contains a single pilot gain. The innermost control loop also contains a second-order "neuromotor" model. The fact that system output, output rate, and input are each assumed available to the human in this description leads to the use of the term "pursuit" pilot model. As will be seen, the rate feedback will be created by a combination of proprioceptive and vestibular information (when the latter is available from vestibular sensors).

In [13], selection of the pilot gains in each control loop is accomplished as follows. Consider Fig. 1 showing the pilot model controlling a single response variable, denoted M in the figure. For example, M might be the pitch attitude (θ) of a rotorcraft. G_{nm} is the second-order neuromotor model alluded to in the previous paragraph and is given by

$$G_{\text{nm}} = \frac{10^2}{s^2 + 2(0.707)10s + 10^2} \tag{1}$$

The gain K_r is chosen so that a 10 dB difference exists between the amplitude of the most-lightly damped mode and the midfrequency amplitude in a Bode plot of the transfer function $\dot{M}/R$. Justification for the 10 dB factor is given in [13]. The gain K_p is then selected to yield a nominal 2 rad/s crossover frequency in the Bode plot of the open-loop M/E transfer function. The 2 rad/s figure is representative of an upper limit of pilot crossover frequency in flight tasks [15].

In multiloop control problems, other response variables must obviously be used by the pilot. For example, if the task at hand was rotorcraft hover control, vehicle longitudinal position (x) might serve as the next response variable, with pitch attitude serving as a command for controlling x. Figure 2 shows, in generic fashion, how such a loop closure would be modeled.

In Fig. 2, the block labeled "vehicle with primary loop closed" actually includes two loop closures, that is, the $\dot{M}$ and M loops from Fig. 1. In the rotorcraft example, M_0 would refer to longitudinal displacement x, and $\dot{M}_0$ would refer to longitudinal velocity. In the approach of [13], the gain K_{ro} is chosen so as to produce the same

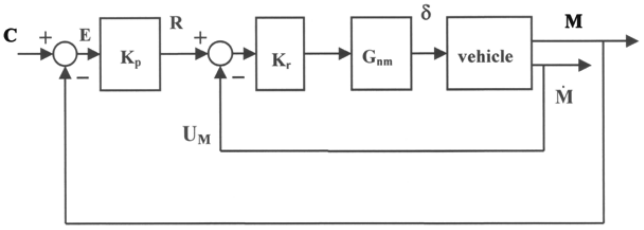

Fig. 1 A model of human pilot control behavior from [13].

crossover frequency in the $\dot{M}_0$ loop as in the primary control loop, here 2 rad/s. The gain K_{po} is then chosen to yield a crossover frequency a factor of 3 less, that is, 0.667 rad/s. The use of a factor of 3 to separate major control loops in a multiloop task has been discussed elsewhere [17]. If further outer-loop closures are required, the procedure outlined is employed again. The rate gain in the next loop would be selected to yield a 0.667 rad/s crossover frequency in that loop, and the position gain would be selected so as to yield a crossover frequency of $0.667/3 = 0.222$ rad/s.

For the applications to be discussed, the model of Fig. 1 is modified so as to allow explicit proprioceptive and vestibular cues. As Fig. 3 indicates, $\dot{M}$ is replaced by a weighted sum of these cues, each providing estimates of the same variable. First an approximation to the transfer function $\dot{M}/\delta$ is obtained and weighted at 0.75. This transfer function is obtained by exciting the system with a filtered step $\delta(t)$ in the control loop in question. A MATLAB m-file is then used to estimate the transfer function between $\dot{M}$ and δ using a regression technique. The lowest order transfer function that provides an acceptable match to $\dot{M}$ given δ is used. Then, if $\dot{M}$ can also be sensed by a vestibular organ (semicircular canals and/or otoliths), this $\dot{M}$ is weighted at 0.25. Note that the two $\dot{M}$ signals have different sources, one is from the control input δ and the second is the signal itself (no models of the vestibular sensors are included). The two resulting signals are summed and fed back into the innermost rate loop. The 0.75/0.25 split is an assertion at this point. Note that if no vestibular organ provides the necessary $\dot{M}$, then only proprioceptive feedback is used and weighted at 1.0. The normalized variable UM/K_{po} will be used to create a fidelity metric (FM) to be described in Sec. II.E.

For any task, the outer-loop command C_O passes through a second-order filter with unity damping ratio and a break frequency defined by [13]

$$\omega_{n\,\text{filter}} = k_{\text{agress}}(2.4 - 0.4f)\ \text{rad/s} \tag{2}$$

The factors k_{agress} and f will be defined in Secs. II.B and II.C, respectively. In Eq. (2), the factor $(2.4 - 0.4f)$ represents the crossover frequency of the innermost rate loop (pitch rate) as a function of f. Equation (2) ensures that the majority of power in the command signal does not exceed the highest bandwidth control loop in the pilot model.

B. Modeling Visual Cue Quality and Pilot Control Aggressiveness

The model for visual cue quality introduced in [6] and used in [13] does not impact the selection of nominal pilot model gains. The gain in each control loop that provides *visual* (as opposed to

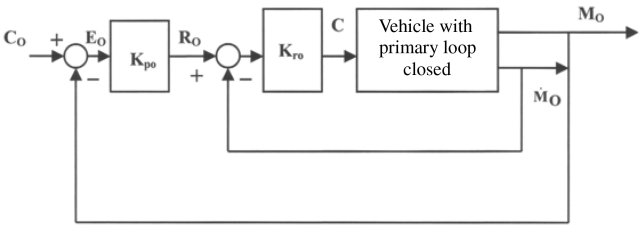

Fig. 2 A multiloop pilot/vehicle system from [13].

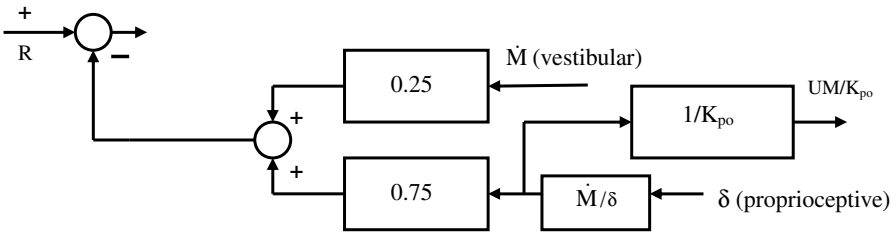

Fig. 3 Creating proprioceptive and vestibular feedback.

proprioceptive or vestibular) feedback is preceded by a visual cue model of the form shown in Fig. 4. Details concerning the model can be found in [13].

The saturation limits in the element in the visual model are set to twice the variance $dvar_{\text{vis}}$ of a zero-mean, normally distributed random variable. A new random number is generated every 0.05 s. The quality of the visual cues is quantified by the $dvar_{\text{vis}}$ value. The larger this value, the poorer the visual cue. For simplicity, this value will be the same for all control loops and, as such, will reflect the average quality of all visual cues. An important part of the model is the gain reduction factor f. The gains on all *rate-control* loops are multiplied by $1/f$ where f will be defined in what follows.

If desired, pilot control aggressiveness can be modeled by a multiplying factor k_{agress} that multiplies the gains in all the outer loops of each pair of loop closures, that is, K_p and K_{po} in Figs. 1 and 2. In [13] it was suggested that a preliminary relationship between $dvar_{\text{vis}}$ and the usable cue environment (UCE) [18] could be given by

$$\begin{aligned} &\text{if } 0 \le dvar_{\text{vis}} < 0.1, \qquad \text{UCE} = 1 \\ &\quad 0.1 \le dvar_{\text{vis}} < 0.2 \qquad \text{UCE} = 2 \\ &\quad 0.2 \le dvar_{\text{vis}} < 0.3, \qquad \text{UCE} = 3 \end{aligned} \tag{3}$$

C. Modeling Task Interference Among Control Axes

Existing human operator tracking data involving multi-axis control indicates that multi-axis tracking induces increased human operator remnant and decreased operator "gain" [19]. In a measurement of human pilot dynamics in a tracking task, remnant is defined as that part of the pilot's control input that is not linearly correlated with the system external forcing function or disturbance [17]. In the current study, this behavior is most easily modeled through the visual cue model. The dependence of the number of axes being controlled and $dvar_{\text{task}}$ will be defined as

$$\begin{aligned} dvar_{\text{task}} &= 0.01n \quad \text{for } n > 1 \\ &= 0 \quad \text{for } n = 1 \end{aligned} \tag{4}$$

where n is the number of axes being controlled. This equation is based upon a limited review of task interference data supplied in [19]. The variable f introduced in Sec. II.B can now be defined as

$$f = 1 + 10(dvar_{\text{vis}} + dvar_{\text{task}}) \tag{5}$$

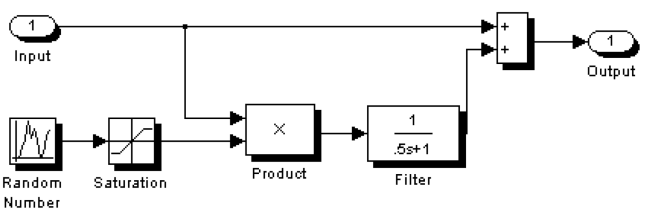

Fig. 4 The visual cue model of [13].

D. Modeling Higher Levels of Skill Development

As described in [5,6], an inverse dynamics element can be included as the final, outermost loop element in the pilot modeling procedure. This element effectively inverts the dynamics of the pilot/vehicle system, as shown in Fig. 5. The inverse dynamics filter is created from linear dynamic inversion [20] applied to the linear pilot/vehicle system. The importance of the filter is that it provides feedforward command cross coupling to the pilot/vehicle system, effectively modeling the skilled pilot's ability to employ such behavior to minimize the effects of control cross coupling in the vehicle dynamics.

E. Assessing Simulator Fidelity

Reference [2] offers a useful definition of training simulator fidelity that forms the basis of the procedure to be used here, that is,

> "We suggest, then, that fidelity is the specific quality of a simulator that permits the skilled pilot to perform a given task in the same way that it is performed in the actual aircraft. Execution of said task is simply the closure of all loops made necessary by both the task requirements and the dynamics of the vehicle and subject to the information which is available."

This definition will be employed in this study as follows: A nominal pilot model will be created for a particular vehicle and task assuming no simulator limitations such as computational time delays, motion system limitations, or degraded visual cues. This model will then be employed in a computer simulation in which such simulator limitations are included. A fidelity metric will be calculated that assesses the degree of fidelity that the simulator would exhibit in this task. The fidelity metric is similar to that used in [5,6], but modified to accommodate the simplified pilot model. The FM is based upon the power $P_i(\omega)$ in the ith normalized signal U_{Mi} in the model of Fig. 1,

$$P_i(\omega) = \frac{1}{K_{p_i}^2}\Phi_{U_{M_i}}(\omega) \tag{6}$$

and

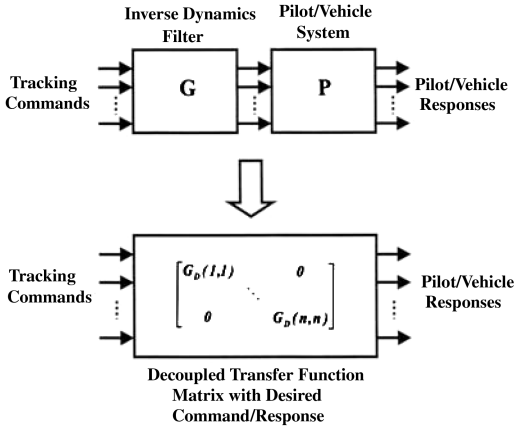

Fig. 5 Inverse dynamics from [6].

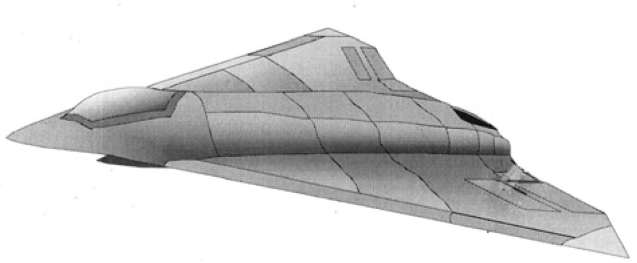

Fig. 6 The innovative control effector (ICE vehicle).

$$\mathrm{FM} = \sum_{i=1}^{n}\left[\frac{\int_0^\infty |P_i(\omega)_{\mathrm{nom}} - P_i(\omega)_{\mathrm{sim}}|\mathrm{d}\omega}{\int_0^\infty P_i(\omega)\mathrm{d}\omega}\right] \tag{7}$$

Here n is, again, the number of axes being controlled by the pilot. Note that if FM $= 0$, perfect fidelity is implied given the definition in the paragraph above.

At least a few words of justification for employing the metric of Eq. (7) are in order. The proprioceptive feedback signal shown in Fig. 3 is the dominant part of the signal that provides the pilot compensation dynamics in each of the fundamental control loops closed by the pilot (e.g., M/R in Fig. 1). Assume, for example, that the pilot is controlling a simple vehicle with dynamics of $1/s^2$. Following the pilot model development that has been described herein, the proprioceptive dynamics would be given by $1/s$. A gain of 8.0 in the forward loop (to provide appropriate closed-loop neuromuscular mode peaking) would then yield a pilot model of the form:

$$Y_p \approx \frac{K_p s}{(s+12.09)(s^2+2(0.13)8.14s+8.14^2)} \tag{8}$$

Over a broad frequency range including typical crossover frequencies for M/E in Fig. 1 (1–2 rad/s), Eq. (8) generates an effective "lead" which not only stabilizes the manual closed-loop system, but also ensures adequate stability margins. Thus, given the importance of the proprioceptive signal in the piloted vehicle system, differences in the frequency-integrated power which accrue when simulator limitations are included in the modeling procedure should serve as sensitive indicators of simulator fidelity.

III. Example: Fighter Aircraft

A. Aircraft and Pilot Model Description

Figure 6 shows the innovative control effector (ICE) vehicle used in other studies [21]. Here the pilot will be tracking random-appearing pitch and roll-attitude commands, emulating a tail-chase scenario. The flight condition is Mach $= 0.3$, altitude 15,000 ft. The aircraft model used here can be found in [21], including the models for amplitude and rate-limited actuators. The aircraft possesses a three-axis stability and command augmentation system described as the "loop-shape" design in [21]. Figure 7 shows the pilot model for this vehicle and task. The innermost loops show both vestibular and proprioceptive feedback as described in Sec. II.A.

The human's vestibular sensors are assumed to provide the angular velocity information [22]. The dynamics of these sensors are not included in the model. Previous research has justified this simplifying assumption, for example, [23]. The transfer functions shown in the proprioceptive loops were obtained from a time-domain regression technique described in Sec. II.A. The pilot model gains and transfer functions for the proprioceptive dynamics in the pilot model are given, respectively, as

$$k_p = 1.07; \quad k_q = 0.7; \quad k_\phi = 3.8369; \quad k_\theta = 7.25$$
$$q \text{ loop}: \frac{2.674s^2 + 10.2s - 0.1983}{s^2 + 13.32s + 2.56} \qquad p \text{ loop}: \frac{0.9245s + 7.437}{s + 7.338} \tag{9}$$

B. Task and Results

The flight task will involve following random-appearing pitch and roll-attitude commands. This task represents a tail-chase scenario in which the ICE vehicle is attempting to match the perceived pitch and roll attitudes of a target aircraft. Figure 8 shows the pilot/vehicle

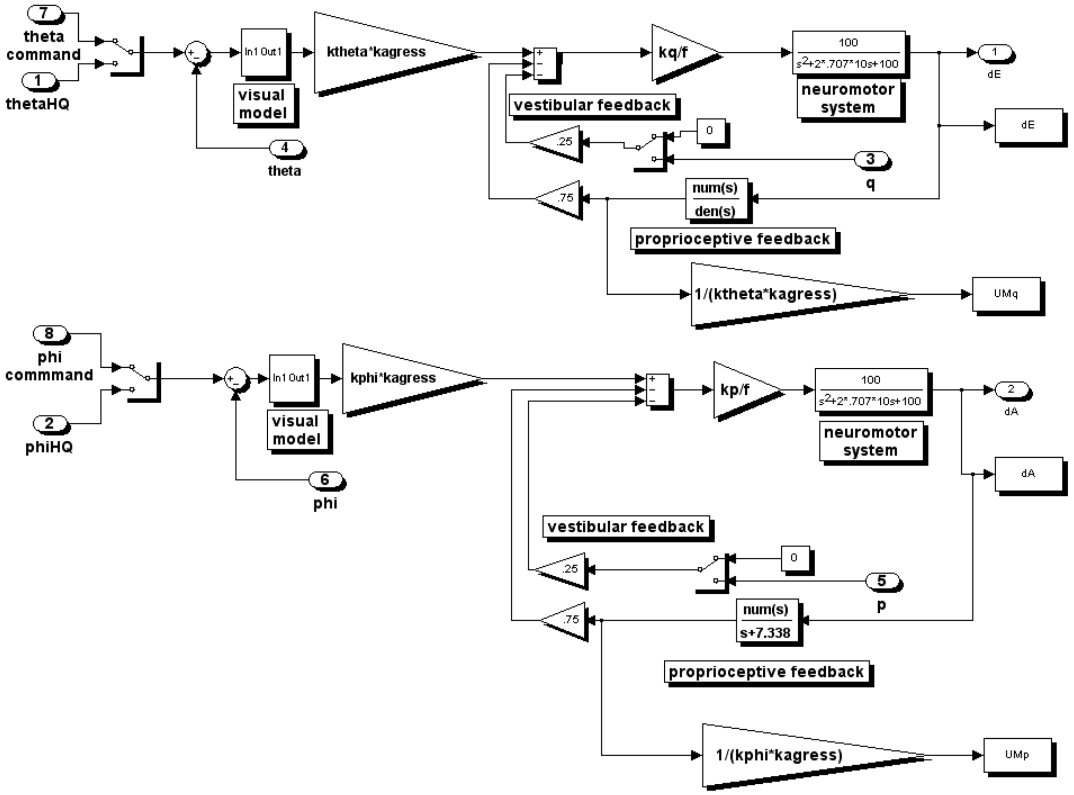

Fig. 7 Pilot model for ICE vehicle.

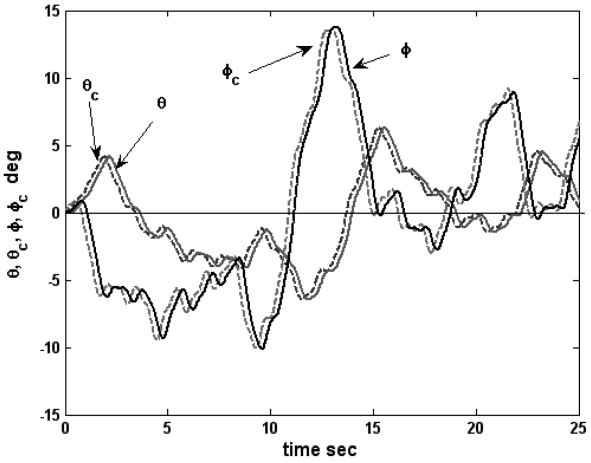

Fig. 8 Pilot/vehicle tracking performance, nominal conditions, ICE vehicle.

performance under nominal conditions, as might be expected from flight data. Tracking performance is seen to be excellent.

The same computer simulation was repeated, but without motion cues. No other changes in the pilot model were undertaken. This would represent placing a skilled pilot in a flight simulator in which no motion cues were present and not allowing the pilot to change any of his/her dynamic characteristics to accommodate simulator limitations. It should be emphasized, of course, that a pilot will likely change his/her dynamics to accommodate differences between the simulator and the actual vehicle in the task at hand. This does not invalidate the methodology. The technique offered is essentially asking what changes in the pilot's sensory signals and performance will occur if the pilot does not change dynamics from those appropriate from the actual vehicle. Figure 9 shows the tracking performance and Figs. 10 and 11 compare the power in the pilot's proprioceptive feedback loops [Eq. (6)] with and without motion cues. These power calculations were obtained from runs of 60 s duration. Power appearing to be concentrated around specific frequencies is attributable to the random-appearing pitch and roll-attitude commands being generated by sums of sinusoids. The reader should be reminded that these results are *task dependent*. Evaluation of Eq. (7) for the pitch and roll FM values indicates

$$\begin{aligned}\text{FM} &= \text{pitch-loop contribution} + \text{roll-loop contribution}\\ &= 0.1 + 0.16 = 0.28\end{aligned} \tag{10}$$

Perfect fidelity would produce an FM = 0. Equation (10) merely states that there was a 28% increase in FM that resulted from the removal of motion cues. At this juncture, mapping a 28% increase in FM to more subjective fidelity assessment is open to question.

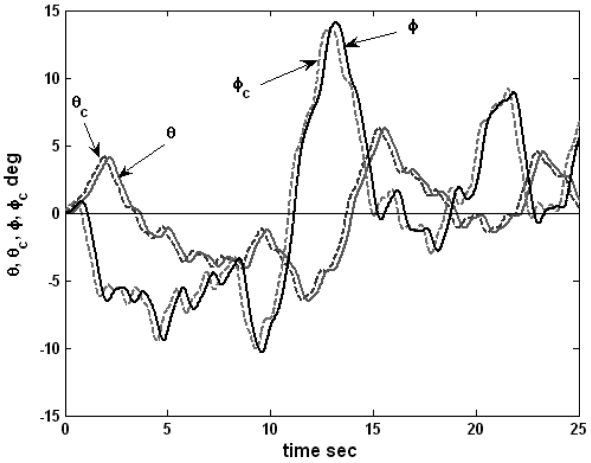

Fig. 9 Pilot/vehicle tracking performance, no motion cues, ICE vehicle.

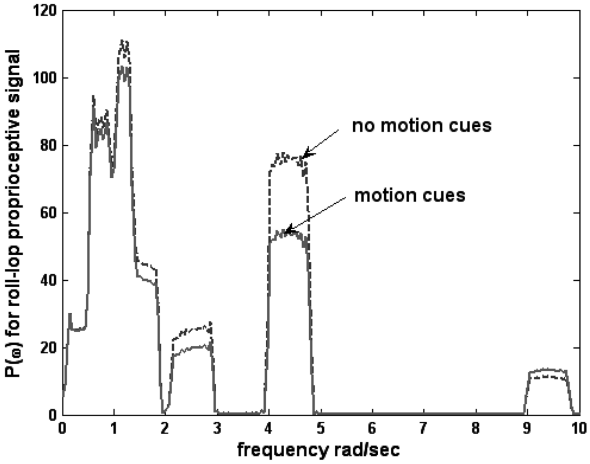

Fig. 10 Power in pilot's pitch-loop proprioceptive signal for ICE-vehicle tracking task.

IV. Example: Small Rotorcraft

A. Aircraft and Pilot Model Description

Figure 12 shows the BO-105 rotorcraft that has been used in other studies [13]. Here the pilot/aircraft system will be performing simple repositioning maneuvers near hover. The pilot is controlling four axes, with the outermost loops controlling longitudinal, lateral, vertical positions, and heading. In addition to vestibular sensing of the angular rate in the pilot model, linear acceleration cues were employed for $\ddot{x}$, $\ddot{y}$, and $\ddot{h}$. It was assumed that the human's vestibular sensors could provide these cues [22]. Again, the dynamics of these sensors were ignored in the model, an assumption justified by previous applications to vehicular control [23]. As implemented in [6], $\ddot{x}$ and $\ddot{y}$ were assumed to provide surrogate attitude cues for θ and ϕ. The visual attitude cues were blended with the vestibular cues according to

$$\theta_{\text{sensed}} = 0.75\theta_{\text{visual}} - 0.25\ddot{x}/g \qquad \phi_{\text{sensed}} = 0.75\phi_{\text{visual}} + 0.25\ddot{y}/g \tag{11}$$

As was the case with blending the proprioceptive and vestibular cues, the 0.75/0.25 split is an assumption.

Figure 13 shows the entire pilot/vehicle system and is included to emphasize the complexity of this modeling exercise. Figure 14 shows the pilot model for longitudinal control. The actuator dynamics given in [13] were modified here to include amplitude and rate limits. Note the added complexity of the model of Fig. 14 compared to either control axis for the ICE pilot model of Fig. 7. This is attributable to the additional control loops in each control axis.

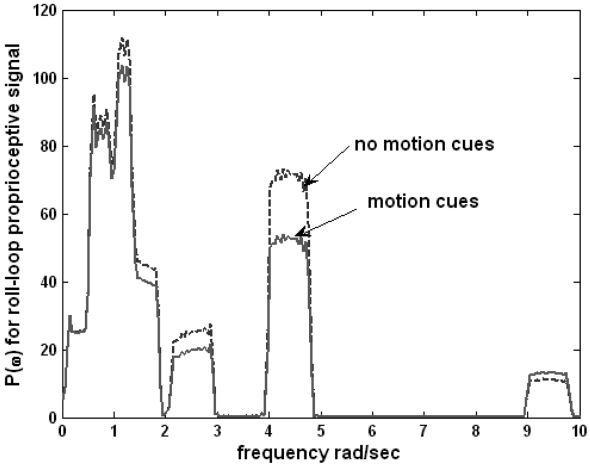

Fig. 11 Power in pilot's roll-loop proprioceptive signal for ICE-vehicle tracking task.

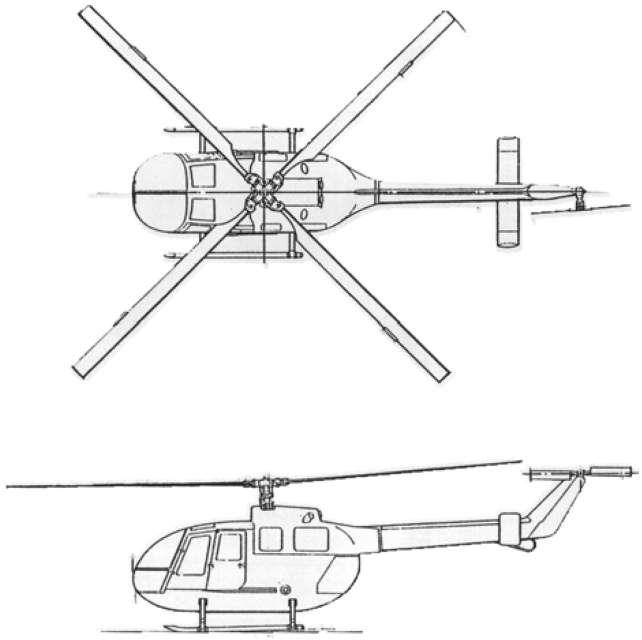

Fig. 12 BO-105 rotorcraft.

The pilot gains and the transfer functions for the proprioceptive dynamics in the pilot model are given, respectively, as

$$k_q = -15.83; \quad k_p = 11.1; \quad k_{\ddot{h}} = 1.12; \quad k_{\dot{r}} = 2.69k_\theta = 2.93$$
$$k_\phi = 3.43; \quad k_{\dot{h}} = 3.39; \quad k_r = 3.35; \quad k_{\dot{x}} = -0.27$$
$$k_{\dot{y}} = 0.25; \quad k_h = 0.73; \quad k_\psi = 0.72; \quad k_x = 0.64; \quad k_y = 0.65$$
$$\ddot{h} \text{ loop}: \frac{10.57s + 0.2056}{s^2 + 7.306s + 3.505} \qquad q \text{ loop}: \frac{-0.222s + 0.03514}{s^2 + 0.8433s + 0.4144}$$
$$p \text{ loop}: \frac{0.44243s - 0.06758}{s^2 + 2.067s + 0.7412} \qquad \dot{r} \text{ loop}: \frac{4.381s + 0.1152}{s^2 + 7.11s + 2.674} \tag{12}$$

The inclusion of gains such as $k_{\ddot{h}}$ and $k_{\dot{r}}$ in Eqs. (12) arises from the basic structure of the pilot model as shown in Fig. 1, in which control of variables such as $\dot{h}$ and r require inner rate loop closures on $\ddot{h}$ and $\dot{r}$. Increased pilot skill level is exercised in this simulation by inclusion of the inverse dynamics system as described in Sec. II.D. Note the block labeled Pilot Skill Level in Fig. 13.

B. Task and Results

The task to be considered will be a simple repositioning task in which the rotorcraft is to translate vertically, laterally, and longitudinally a distance of 10 m and return to hover. After hovering for approximately 10 s, the vehicle translates back to the original vertical and lateral positions, but longitudinally 20 m from its

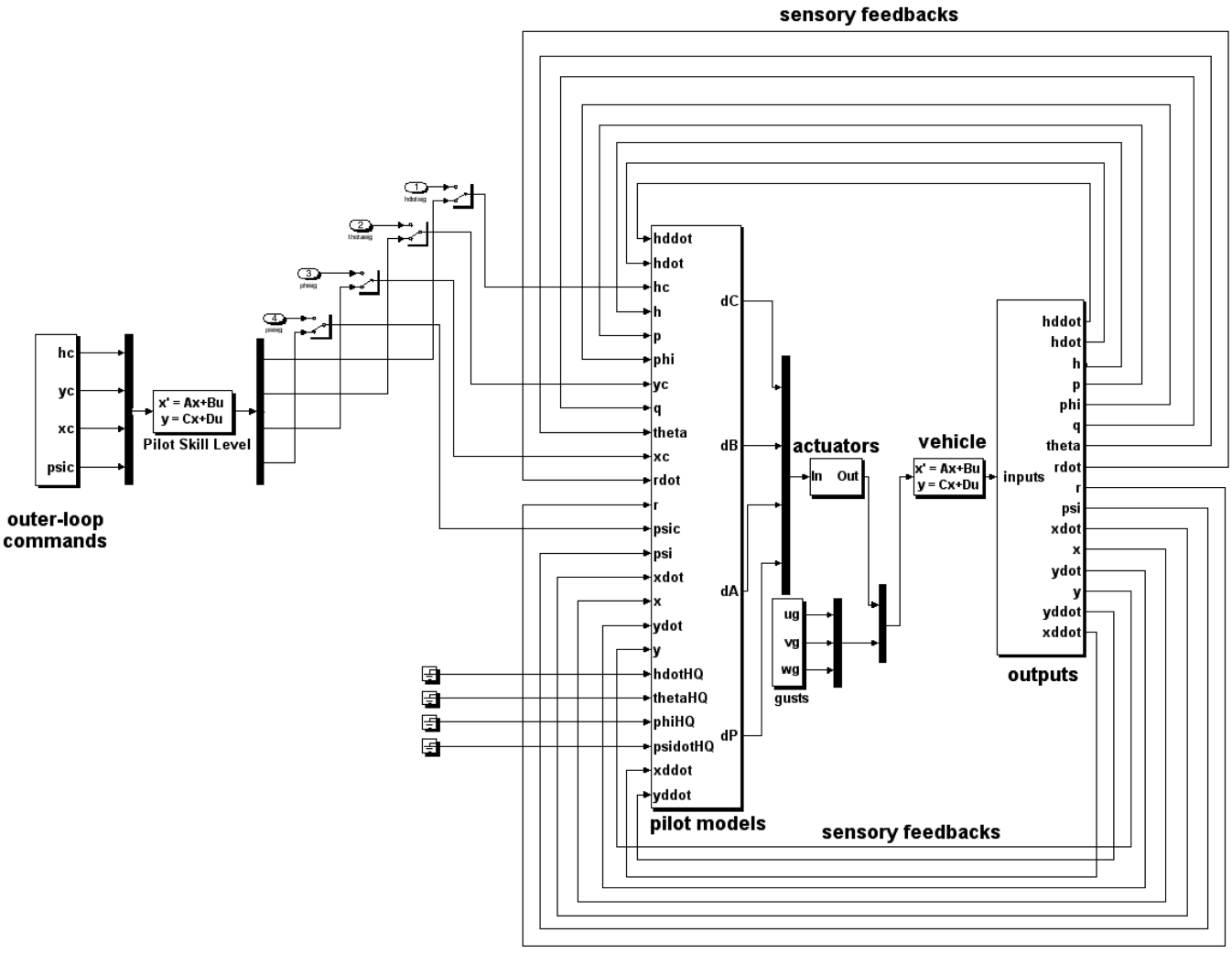

Fig. 13 Pilot/vehicle system for rotorcraft task modeling.

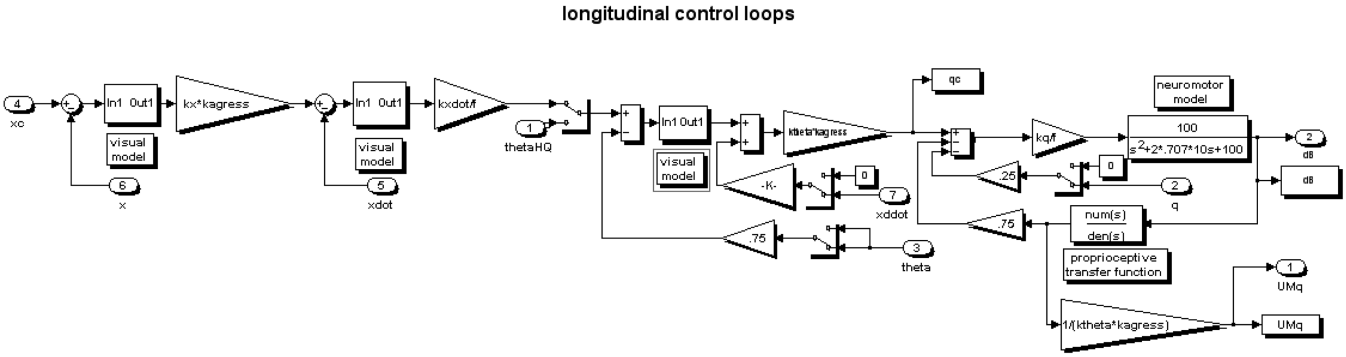

Fig. 14 Longitudinal pilot model for rotorcraft task modeling.

original longitudinal position. During the maneuver, the desired heading deviation is zero. Turbulence inputs were included and modeled as white noise passed through second-order filters with 5 rad/s bandwidths creating body-fixed velocity perturbations u_g, v_g, and w_g. The rms turbulence values were 1 m/s in each axis. Figure 15 shows the vehicle position and heading performance under nominal conditions, again as might be expected from flight data.

The same computer simulation was repeated, but without motion cues. No other changes in the pilot model were undertaken. As in the case of the ICE-vehicle simulation, this would represent placing a skilled pilot in a flight simulator in which no motion cues were present and not allowing the pilot to change any of his/her dynamic characteristics to accommodate simulator limitations. Figure 16 shows the tracking performance. Some performance degradation is evident, particularly in heading control. Figures 17–20 compare the power in the pilot's proprioceptive feedback loops [Eq. (6)] with and without motion cues.

The graphical results suggest that roll-rate motion cueing is most important in this task. This is further corroborated by the roll-loop's contribution to the FM in Eq. (13). One explanation for this result lies in the control cross coupling that exists for this vehicle at hover. The ratio $L'_{\delta_B}/M_{\delta_B} \cong -0.5$, whereas $M_{\delta_A}/L'_{\delta_A} \cong 0.06$. This implies that roll disturbances due to longitudinal cyclic inputs by the pilot will be considerably larger than pitch disturbances due to lateral cyclic inputs. Again, the reader should be reminded that these results are task dependent. Evaluation of Eq. (7) for the pitch and roll FM values were obtained for 40 s runs. These indicate

$$\begin{aligned}\text{FM} &= \text{pitch-loop contribution} + \text{roll-loop contribution}\\ &\quad + \text{vertical position-loop contribution}\\ &\quad + \text{heading-loop contribution}\\ &= 1.36 + 2.39 + 0.36 + 0.837 = 4.95\end{aligned} \tag{13}$$

The coarse nature of the motion/no-motion dichotomy can be made finer by considering motion cues, but with washout and gain limitations included in the motion drive systems. To this end, motion system dynamics from [6] were used, expanded upon, and defined (in shorthand notation) by

$$\begin{gathered}\text{vertical axis}: \ 0.8(0)^2/[0.707, 0.3]\\ \text{lateral axis}: \ 0.5(0)^2/[0.707, 0.5] \quad \text{pitch axis}: \ 0.4(0)^2/[0.707, 0.5]\\ \text{roll axis}: \ 0.48(0)^2/[0.707, 0.5] \quad \text{yaw axis}: \ 0.5(0)^2/[0.707, 0.5]\end{gathered} \tag{14}$$

The shorthand notation in Eqs. (14) is defined as $a(b)/[c, d] = a(s + b)/[s^2 + 2(c)(d)s + d^2]$. These transfer functions are defined as (x-cockpit motion/x-vehicle motion). These dynamics do not represent any particular motion system, however, the gains and washout frequencies would be representative of a "large motion" facility. Figure 21 shows the pilot vehicle performance. Comparison with the performance shown in Figs. 15 and 16 reveals that performance is approaching that of the full-motion (flight) results. For the sake of brevity, no graphical comparisons of the $P(\omega)$ plots will be presented, but the fidelity metric of Eq. (7) is calculated as

$$\begin{aligned}\text{FM} &= \text{pitch-loop contribution} + \text{roll-loop contribution}\\ &\quad + \text{vertical position-loop contribution}\\ &\quad + \text{heading-loop contribution}\\ &= 0.4 + 0.7 + 0.05 + 0.15 = 1.30\end{aligned} \tag{15}$$

Comparing the FMs of Eqs. (13) and (15) indicates that significantly improved fidelity is obtained with the limited motion systems described in Eqs. (14).

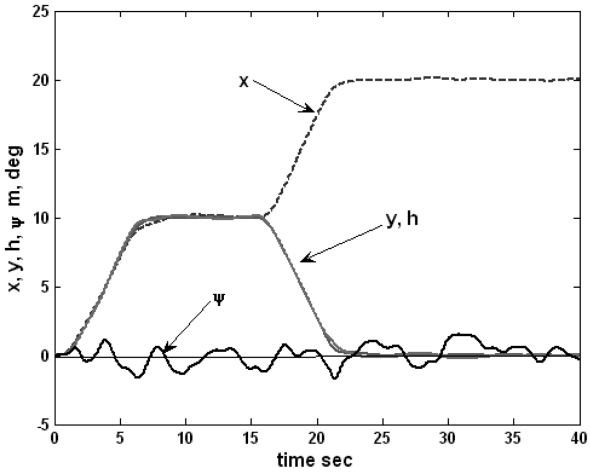

Fig. 15 Pilot/vehicle tracking performance, nominal conditions, BO-105 vehicle.

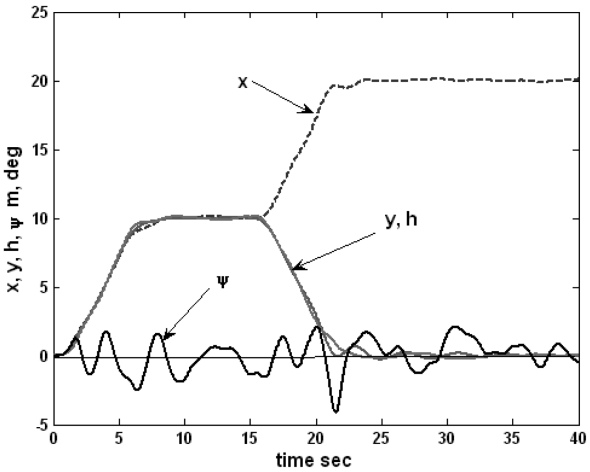

Fig. 16 Pilot/vehicle tracking performance, no motion cues, BO-105 vehicle.

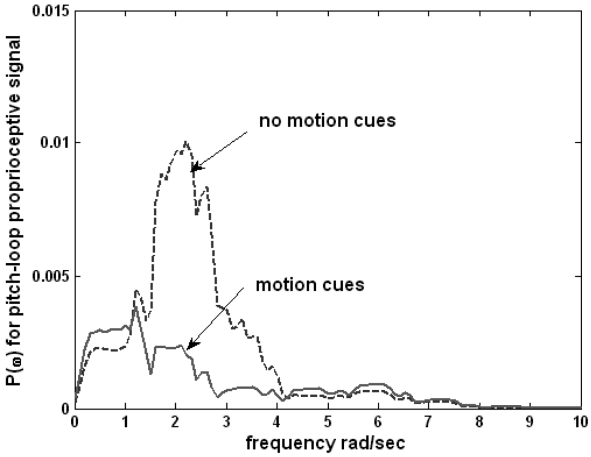

Fig. 17 Power in pilot's pitch-loop proprioceptive signal for BO-105 vehicle repositioning task.

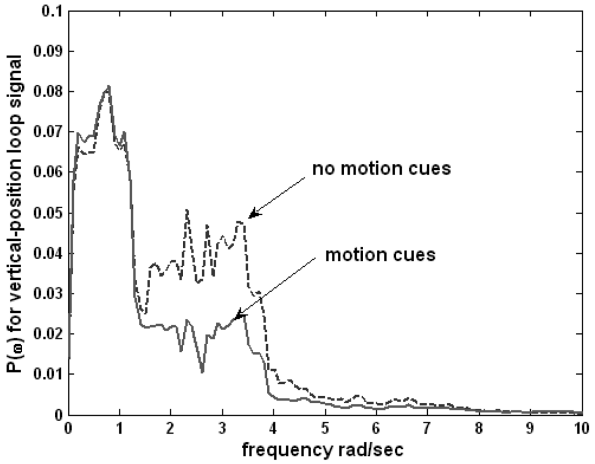

Fig. 19 Power in pilot's vertical-position loop proprioceptive signal for BO-105 vehicle repositioning task.

The next comparison involves the limited motion system just described, but with a degraded visual system, which can be considered to model a limited visual system in the simulator. This will be implemented in the visual cue model by setting $dvar_{\text{vis}} + dvar_{\text{task}} = 0.14$ and $f = 2.4$. Figure 22 shows tracking performance which is the poorest of the three systems that have been simulated. The fidelity metric for this system was found to be

$$\begin{aligned}\text{FM} &= \text{pitch-loop contribution} + \text{roll-loop contribution} \\ &\quad + \text{vertical position-loop contribution} \\ &\quad + \text{heading-loop contribution} \\ &= 0.89 + 1.28 + 0.22 + 0.62 = 3.01 \end{aligned} \tag{16}$$

The final comparison will include the limited motion system, the degraded visual system, plus a 0.05 s time delay in the vehicle model. The time delay can be considered to model computational delays in the host computer for the simulator, and, as such, represents a vehicle modeling error. Figure 23 shows tracking performance which is clearly the poorest of all the systems that have been simulated. The fidelity metric for this system was found to be

$$\begin{aligned}\text{FM} &= \text{pitch-loop contribution} + \text{roll-loop contribution} \\ &\quad + \text{vertical position-loop contribution} \\ &\quad + \text{heading-loop contribution} \\ &= 0.98 + 2.04 + 0.208 + 0.07 = 3.30 \end{aligned} \tag{17}$$

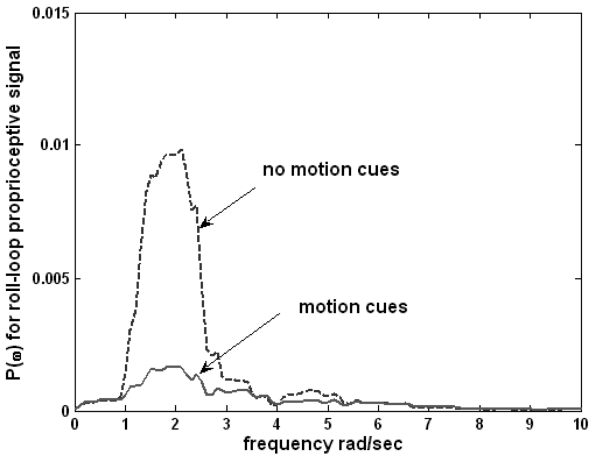

Fig. 18 Power in pilot's roll-loop proprioceptive signal for BO-105 vehicle repositioning task.

The addition of the 0.05 s time delay is seen to result in an approximate 10% reduction in fidelity (an approximate 10% increase in FM).

V. Large Rotorcraft

A. Aircraft and Pilot Model Description

The final example involves the large rotorcraft shown in Fig. 24, the CH-53D. The vehicle model was created by a linear interpolation of the vehicle stability derivatives as given in [24] over an airspeed range from hover to 120 kt. Thus, the vehicle model is linear but time varying in nature. Stability augmentation systems were included in each axis providing attitude command/attitude hold in pitch and roll, and rate command in the vertical and yaw axes. As in the example of the previous section, the pilot is controlling four axes. As opposed to the modeling of Sec. IV, the outermost loops control longitudinal, lateral, vertical velocities, and heading rate. The pilot model was formulated using the hover dynamics of the vehicle. For simplicity, no dynamic inversion element was included in the pilot model. Finally, the pitch-attitude commands created by the pilot model were limited to ± 30 deg in the simulation.

To accommodate the time-varying vehicle dynamics it was necessary to schedule the pilot gains in the forward portion of the vertical control loops (those controlling $\dot{h}$ and $\ddot{h}$). This was accomplished by adjusting the nominal gain values with airspeed as follows:

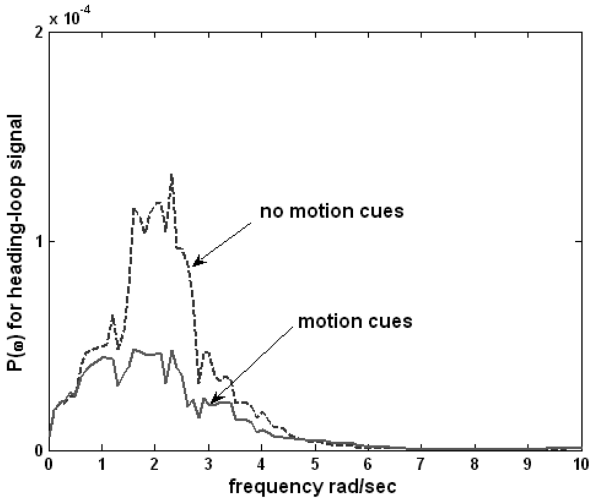

Fig. 20 Power in pilot's heading-loop proprioceptive signal for BO-105 vehicle repositioning task.

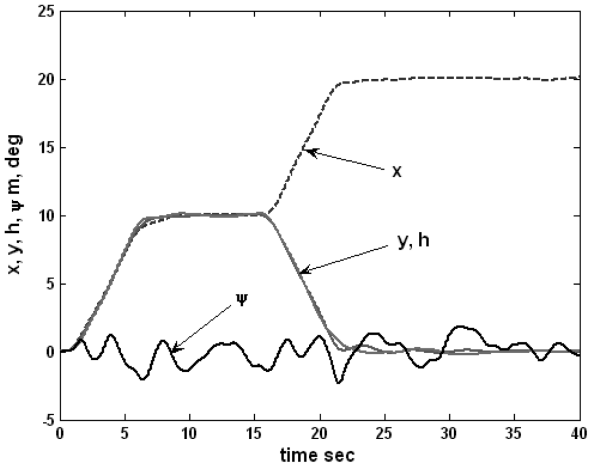

Fig. 21 Pilot/vehicle tracking performance, reduced motion cues, BO-105 vehicle.

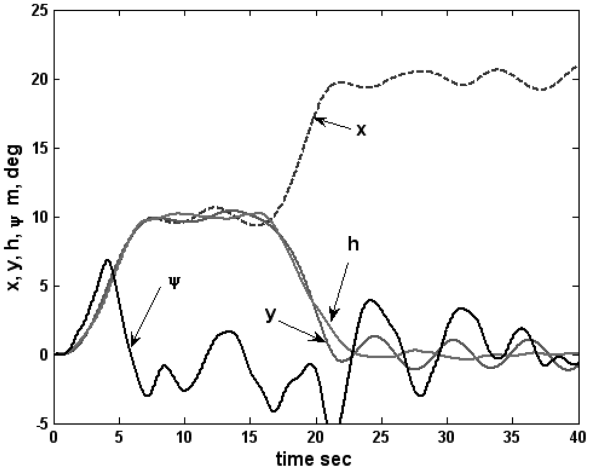

Fig. 23 Pilot/vehicle tracking performance, reduced motion cues, degraded visual cues, and computational time delay BO-105 vehicle.

$$
\begin{aligned}
k_{\ddot{h}} &= 12 \quad \text{for } V < 100 \text{ ft/s} \\
k_{\ddot{h}} &= \frac{12}{1 + 0.125(V - 100)} \quad \text{for } V \geq 100 \text{ ft/s} \\
k_{\dot{h}} &= 2.34 \quad \text{for } V < 100 \text{ ft/s} \\
k_{\dot{h}} &= \frac{2.34}{1 + 0.125(V - 100)} \quad \text{for } V \geq 100 \text{ ft/s}; \qquad V = \text{airspeed}
\end{aligned} \tag{18}
$$

The pilot model gains and transfer functions for the proprioceptive dynamics in the pilot model are given, respectively, as

$$
\begin{aligned}
&k_p = 0.8; \quad k_q = 0.875; \quad k_\phi = 3.23; \quad k_\theta = 2.91; \quad k_{\ddot{h}} = 12 \\
&k_{\dot{r}} = 3.3; \quad k_{\dot{y}} = 0.00922; \quad k_{\dot{x}} = -0.0319; \quad k_{\dot{h}} = 2.34 \\
&k_r = 2.36 \quad \ddot{h} \text{ loop}: \frac{0.514s}{s + 0.5188} \quad q \text{ loop}: \frac{2.948s - 0.08813}{s + 1.756} \\
&p \text{ loop}: \frac{3.562s - 0.0325}{s + 3.102} \quad \dot{r} \text{ loop}: \frac{2.48s + 0.00187}{s + 2.525}
\end{aligned} \tag{19}
$$

The values shown for $k_{\ddot{h}}$ and $k_{\dot{h}}$ are valid for $V = 100$ ft/s. British gravitational (BG) units, as opposed to SI units are employed in the following examples because reference is made to task descriptions in [25] that employ BG units.

B. Tasks and Results

Acceleration/Deceleration Task: The task to be considered will be a simple longitudinal acceleration/deceleration maneuver in which the rotorcraft is to accelerate to approximately 110 kt (185.6 ft/s) then decelerate to hover. The reader should note that this task differs somewhat from the "acceleration/deceleration" task described in [25]. Here, a higher velocity was employed before the deceleration segment was initiated. No turbulence inputs were included. Figure 25 shows the vehicle longitudinal velocity tracking performance, including pitch and roll-attitude excursions under nominal conditions, again as might be expected from flight data. Figure 26 compares the power in the roll-loop proprioceptive signals. For the sake of brevity, only the power in this loop is shown. With no turbulence inputs, the spectra have a more limited frequency range, as a comparison of the abscissa of Fig. 26 to those of the previous vehicle examples.

Evaluation of Eq. (7) for the pitch, roll, vertical velocity, and heading-rate loops FM values were obtained for 75 s runs. These indicate

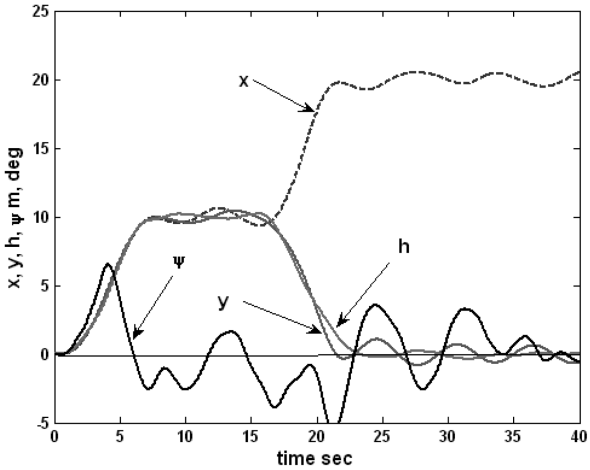

Fig. 22 Pilot/vehicle tracking performance, reduced motion cues and degraded visual cues, BO-105 vehicle.

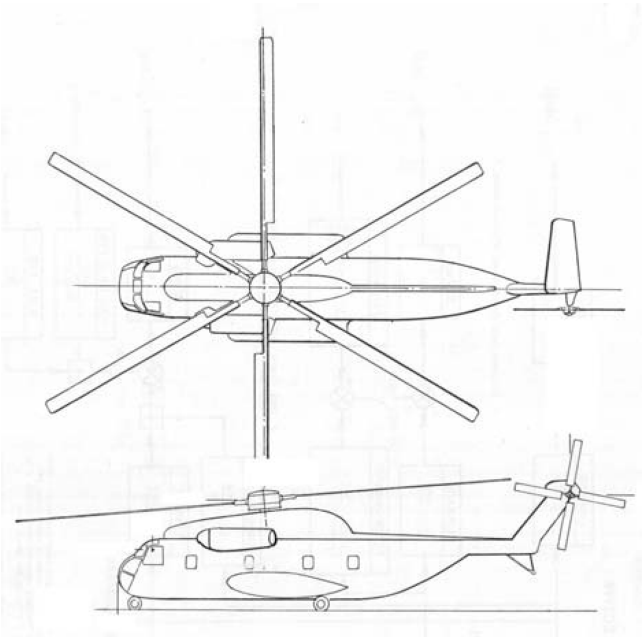

Fig. 24 CH-53D rotorcraft.

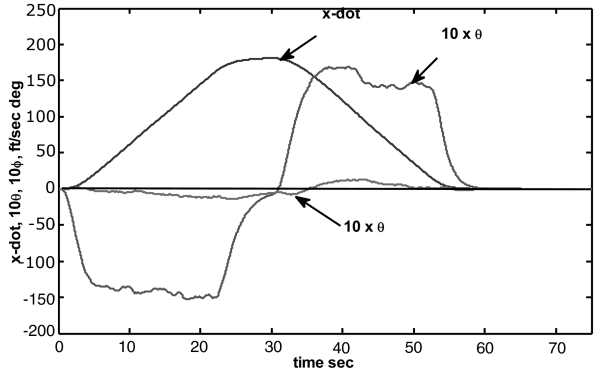

Fig. 25 Pilot/vehicle tracking performance, acceleration/deceleration task, nominal conditions, CH-53D vehicle.

$$\text{FM} = \text{pitch-loop contribution} + \text{roll-loop contribution} + \text{vertical velocity-loop contribution} + \text{heading-rate loop contribution} = 0.00566 + 0.0277 + 0.122 + 0.0308 = 0.186 \quad (20)$$

Departure/Abort Task: The task to be considered will be a departure/abort task as described in [25]. The vehicle will accelerate from hover to approximately 45 kt (departure); the pilot (model) will then abort the departure by rapidly returning to a hover condition. Again, no turbulence inputs were included. No changes in the pilot model parameters were made from the acceleration/deceleration task, except for the addition of logic to mimic the pilot's sensing when a velocity of 45 kt was reached in the departure. The pilot/vehicle task performance called out for this maneuver in [25] includes "target" pitch attitudes of ± 20 deg; target maneuver endpoint 800 ft from initiation of departure point. . . . It is not permitted to overshoot the intended endpoint and move back. . . . If the rotorcraft stopped short, the maneuver is not complete until it is within 20 ft of the intended endpoint. The simulated vehicle exhibited -15 to 24 deg attitude excursions and came to rest 797 ft from the initiation point. Figure 27 shows the vehicle longitudinal velocity tracking performance, including pitch and roll-attitude excursions under nominal conditions, again as might be expected from flight data.

Evaluation of Eq. (7) for the pitch, roll, vertical velocity, and heading-rate loops FM values were obtained for 30 s runs. These indicate

$$\text{FM} = \text{pitch-loop contribution} + \text{roll-loop contribution} + \text{vertical velocity-loop contribution} + \text{heading-rate loop contribution} = 0.00875 + 0.0269 + 0.0761 + 0.0658 = 0.178 \quad (21)$$

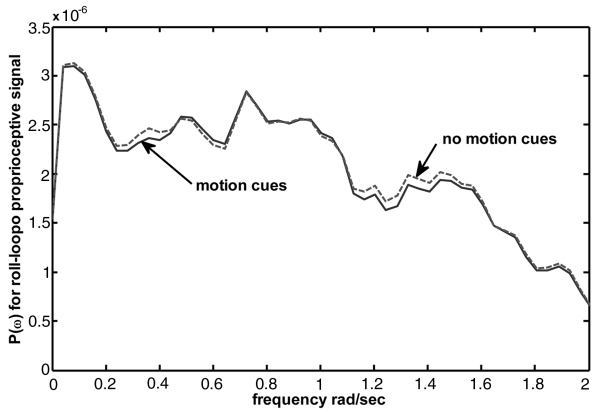

Fig. 26 Power in pilot's roll-loop proprioceptive signal, acceleration/deceleration task, CH-53D vehicle.

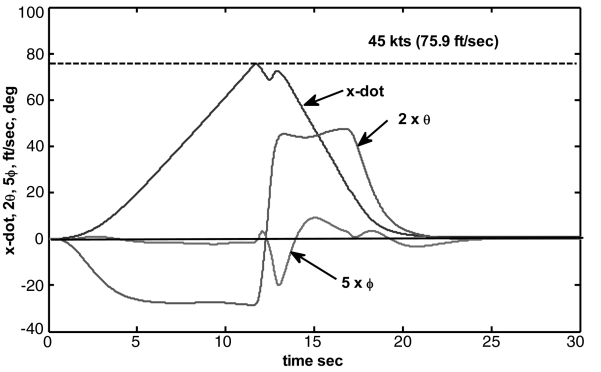

Fig. 27 Pilot/vehicle tracking performance, departure/abort task, nominal conditions, CH-53D vehicle.

Both FM values for the CF-53D are relatively small (suggesting high fidelity). One could argue that the insensitivity to motion cues is attributable to the size of the vehicle.

VI. Discussion and Critique

As a comparison of the FM values among the ICE-vehicle tracking task, the BO-105 vehicle repositioning task and the CH-53D acceleration/deceleration tasks would indicate that the BO-105 rotorcraft and task is considerably more sensitive to simulator motion limitations than the fighter aircraft and large rotorcraft, at least for the vehicles and tasks considered here. This difference can be attributed to both vehicle and task. With its soft, in-plane rigid rotor, the BO-105 is highly maneuverable, and the inherent control cross coupling requires the pilot's use of motion cues to complete the demanding, near-hover task. Finally, as opposed to the BO-105, both the ICE vehicle and the CH-53D possessed stability augmentation systems, the purpose of which was to relieve the pilot's workload. It is worth repeating the definition of fidelity given in Sec. II.E, that is, ". . .the specific quality of a simulator that permits the skilled pilot to perform a given task in the same way that it is performed in the actual aircraft. Execution of said task is simply the closure of all loops made necessary by both the task requirements and the dynamics of the vehicle and subject to the information which is available."

Other than to describe an FM $= 0$ as implying "perfect fidelity," no attempt has been made to assign degrees of "permissible" fidelity to the numerical fidelity metric values that have been obtained in the examples of Sec. IV. For example, is an FM $= 2$ acceptable for a training simulator? At this juncture, the question must remain unanswered and obviously remains an open issue with the modeling procedure. The relative effects of different simulator limitations upon predicted fidelity could be obtained, with the ability to discern the extent to which each axis of control contributes to fidelity or lack of it.

There have been a number of modeling assumptions that were made simply for expediency. Among these were the 0.75/0.25 signal weightings used in several places in the pilot model. In addition, relating ranges in $dvar_{\text{vis}}$ values to specific useable cue environments was based upon relatively crude arguments in [13]. In addition, it is not possible to accurately adjust the $dvar_{\text{vis}}$ values to reflect subtle changes that might accrue in simulator characteristics such as varying visual field of view. One can, of course, reason that reductions in field of view can be accommodated in the model by increases in $dvar_{\text{vis}}$ values, but precisely how large an increase is open to question. This is attributable to the fact that, at the physiological level, the model is egregiously oversimplified. Finally, of course, the modeling procedure has been conducted in the absence of corroborative data involving pilot-in-the-loop simulation. The modeling assumptions outlined in the previous paragraph obviously need to be validated using such data. It is important to note, however, that the pilot model that has been developed follows the dictates of the "crossover model" of the human pilot [13,14].

It was demonstrated in [14] that pilot model parameters for all the vehicles studied here could be selected on the basis of computer simulation of the vehicle. This implied that nonlinear vehicle models, such as those typically used in piloted simulation studies, could be

used to determine the pilot model parameters. The only possible exception to this in the current implementation is the dynamic inversion element discussed in Sec. II.D, which requires a linear vehicle model (as implemented herein). In applications where such a model is unavailable, the recommendation would be to simply omit this element in the modeling procedure.

With these limitations in mind, the possible contribution of the modeling procedure is that it allows predictions of the impact of flight simulator limitations on perceived fidelity as reflected in metrics derived from a tractable control-theoretical pilot model. This model can provide estimates of pilot/vehicle performance in a variety of tasks with a variety of vehicle models. Finally, a procedure has been outlined in [13] and extended herein that allows the user to create the pilot model using a series of well-defined steps.

VII. Conclusions

A tractable pilot modeling procedure is offered that permits computer simulation of realistic flight tasks. The procedure extends a simplified pursuit tracking model of the human pilot previously discussed in the literature. In approximate fashion, the model can account for the effects of task interference, degraded motion and visual cues, vehicle modeling errors, differing levels of pilot control aggressiveness, and to a limited extent, pilot skill level. A fidelity metric similar to one previously discussed in the literature can be offered that predicts, in approximate fashion, the effects of flight simulator limitations on the fidelity of the simulation.

Acknowledgment

The research reported herein was supported by NASA Ames Cooperative Agreement NNX07AR38A, funded under the NASA Subsonic Rotary Wing Project. Barbara Sweet serves as the grant technical manager.

References

[1] Curry, R. E., Hoffman, W. C., and Young, L. R., "Pilot Modeling for Manned Simulation," Vol. I, Air Force Flight Dynamics Lab., AFFDL-TR-76-124, 1976.

[2] Heffley, R. K., Clement, W. F., Ringland, R. F., Jewell, W. F., Jex, H. R., McRuer, D. T., and Carter, V. E., "Determination of Motion and Visual System Requirements for Flight Training Simulators," U.S. Army Research Institute for the Behavioral and Social Sciences, TR 546, Aug. 1981.

[3] Hess, R. A., and Malsbury, T., "Closed-Loop Assessment of Flight Simulator Fidelity," *Journal of Guidance, Control, and Dynamics*, Vol. 14, No. 1, 1991, pp. 191–197. doi:10.2514/3.20621

[4] Hess, R. A., Malsbury, T., and Atencio, A., Jr., "Flight Simulator Fidelity Assessment in a Rotorcraft Lateral Translation Maneuver," *Journal of Guidance, Control, and Dynamics*, Vol. 16, No. 1, 1993, pp. 79–85. doi:10.2514/3.11430

[5] Zeyada, Y., and Hess, R. A., "Human Pilot Cue Utilization with Applications to Simulator Fidelity Assessment," *Journal of Aircraft*, Vol. 37, No. 4, 2000, pp. 588–597. doi:10.2514/2.2670

[6] Hess, R. A., and Siwakosit, W., "Assessment of Flight Simulator Fidelity in Multiaxis Tasks Including Visual Cue Quality," *Journal of Aircraft*, Vol. 38, No. 4, 2001, pp. 607–614. doi:10.2514/2.2836

[7] Johnson, E., and Pritchett, A. R., "Generic Pilot and Flight Control Model for Use in Simulation Studies," AIAA Paper 2002-4694, 2002.

[8] Hosman, R., Schuring, J., and van der Geest, P., "Pilot Model Development for the Manual Balked Landing Maneuvre," AIAA Paper 2005-5884, 2005.

[9] Mulder, M., Kaljouw, W. J., and van Paassen, M. M., "Parameterized Multi-Loop Model of Pilot's Use of Central and Peripheral Visual Motion Cues," AIAA Paper 2005-5894, 2005.

[10] Nieuwenhuizen, F. M., Zaal, P. M. T., Mulder, M., and van Paassen, M. M., "A New Multi-Channel Pilot Model Identification Method for Use in Assessment of Flight Simulator Fidelity," AIAA Paper 2006-6629, 2006.

[11] Zaychik, K. B., Cardullo, F. M., and George, G., "A Conspectus of Operator Modeling: Past, Present and Future," AIAA Paper 2006-6625, 2006.

[12] van den Berg, P., Zaal, P. M. T., Mulder, M., and van Paassen, M. M., "Conducting Multi-Modal Pilot Model Identification—Results of a Simulator Experiment," AIAA Paper. 2007-6892, 2007.

[13] Hess, R. A., "Simplified Approach for Modelling Pilot Pursuit Control Behaviour in Multi-Loop Flight Control Tasks," Institution of Mechanical Engineers, Pt. G, *Journal of Aerospace Engineering*, Vol. 220, No. G2, 2006, pp. 85–102.

[14] Hess, R. A., "Obtaining Multi-Loop Pursuit-Control Pilot Models from Computer Simulation," Institution of Mechanical Engineers, Pt. G, *Journal of Aerospace Engineering*, Vol. 222, No. G2, 2008, pp. 189–200.

[15] Hess, R. A., "Unified Theory for Aircraft Handling Qualities and Adverse Aircraft-Pilot Coupling," *Journal of Guidance, Control, and Dynamics*, Vol. 20, No. 6, 1997, pp. 1141–1148. doi:10.2514/2.4169

[16] Heffley, R. K., Bourne, S. M., Mitchell, D., and Hess, R. A., "Pilot Behavioral Modeling for Flight Operations Near Ships," RHE-NAV-TR-2007-1, Robert Heffley Engineering, 2007.

[17] Hess, R. A., "Feedback Control Models—Manual Control and Tracking," *Handbook of Human Factors and Ergonomics*, edited by G. Salvendy, 2nd ed., Wiley, New York, 1997, Chap. 38.

[18] Hoh, R. H., and Mitchell, D. G., "Handling Qualities Specification—A Functional Requirement for the Flight Control System," *Advances in Flight Control*, edited by M. K. Tischler, Taylor and Francis, London, 1996, Chap. 1.

[19] Levison, W. H., Elkind, J. I., and Ward, J. L., "Studies of Multivariable Manual Control Systems; A Model for Task Interference," NASA CR-1746, 1971.

[20] Stevens, B. L., and Lewis, F. L., *Aircraft Control and Simulation*, 2nd ed., Wiley, Hoboken, NJ, 2003, Chap. 5.

[21] Hess, R. A., Vetter, T. K., and Wells, S. R., "Design and Evaluation of a Damage-Tolerant Flight Control System," Institution of Mechanical Engineers, Pt. G, *Journal of Aerospace Engineering*, Vol. 219, No. G4, 2008, pp. 341–360.

[22] Young, L. R., "Spatial Orientation," *Principles and Practice of Aviation Psychology*, edited by P. S. Tsang, and M. A. Vidulich, Erlbaum, Mahwah, NJ, 2003, Chap. 3.

[23] Hess, R. A., "A Model for the Human's Use of Motion Cues in Vehicular Control," *Journal of Guidance, Control, and Dynamics*, Vol. 13, No. 3, 1990, pp. 476–482. doi:10.2514/3.25360

[24] Heffley, R. K., Jewell, W. F., Lehman, J. M., and Van Winkle, R. A., "A Compilation and Analysis of Helicopter Handling Qualities Data, Vol. 1: Data Compilation," NASA CR-3144, 1979.

[25] Anon., "Aeronautical Design Standard, Performance Specification, Handling Qualities Requirements for Military Rotorcraft," ADS-33E-PRF, U.S. Army Aviation and Missile Command, Aviation Engineering Directorate, Redstone Arsenal, AL, 2000.